Journal of Power Sources 197 (2012) 28–37

Contents lists available at SciVerse ScienceDirect

Journal of Power Sources

journal homepage: www.elsevier.com/locate/jpowsour

Electronic states of metal (Cu, Ag, Au) atom on CeO_2(1 1 1) surface: The role of local structural distortion

Yuanhao Tang[a,b], Hua Zhang[a], Lixia Cui[a], Chuying Ouyang[c], Siqi Shi[a,b,*], Weihua Tang[a], Hong Li[b], Liquan Chen[b]

[a] Department of Physics, Center for Optoelectronics Materials and Devices, Zhejiang Sci-Tech University, Xiasha College Park, Hangzhou 310018, China
[b] Renewable Energy Laboratory, Institute of Physics, Chinese Academy of Sciences, Beijing 100190, China
[c] Department of Physics, Jiangxi Normal University, Nanchang 330022, China

ARTICLE INFO

Article history:
Received 18 August 2011
Received in revised form
11 September 2011
Accepted 12 September 2011
Available online 16 September 2011

Keywords:
Ceria surface
Metal atom adsorption
Structural distortion
Electronic states
First-principles calculations

ABSTRACT

Surface structures and electronic states of metal (M = Cu, Ag and Au) adsorbed on CeO_2(1 1 1) surface have been investigated using first-principles density-functional theory calculations with the on-site Coulomb interaction taken into account. Results indicate that the adsorption is accompanied by an electron charge transfer between neutral metal atom and neighboring Ce^{4+} cation. Charge redistribution with electron localized on the various Ce cations neighboring to adsorbed atom is observed and can be attributed to local structural distortion effects. For the same adsorption site, the structural configuration with the electron localized on the surface Ce cation away from the adsorbed metal atom M is energetically favorable. The strongest adsorption interaction for Cu and Ag is located at 3-fold subsurface O-top site, whereas 2-fold surface O-bridge site is the most stable for Au adsorption. The order on the adsorption energy follows the sequence of Cu > Ag > Au, indicating that Cu atom has a stronger interaction with CeO_2(1 1 1) surface than Ag and Au. Previous controversies about the localization of the transferred electron and the valence state of the adsorbed Au atom have been successfully clarified via analysis of the local structural distortions.

1. Introduction

Ceria-based oxides have been regarded as one of the most important components in many catalytic systems due to their unique properties and extensive applications as active supports in metal-based catalysts for oxidation reactions [1]. These applications are mainly based on the fact that ceria can act as an oxygen reservoir by releasing/uptaking oxygen through the redox processes of the Ce^{4+}/Ce^{3+} couple [2–4] and the strong interactions between metal atom and ceria support. For example, increasing the number and mobility of oxygen vacancies enhances the OSC and correspondingly improves the catalytic activity [5,6]. The reducibility and catalytic activity of CeO_2 are significantly enhanced by the presence of a small amount of transition metal atoms, i.e., Cu, Ag, and Au. However, to date, basic issues, such as the stable adsorption sites and the electronic states at M/CeO_2 (M = Cu, Ag, Au) interfaces remain open. Especially a clarification of the charge state of Au atom on stoichiometric CeO_2(1 1 1) surface is urgently needed, which is one of the aims of the present work.

Associated with this, the Cu/CeO_2 system has been identified as an excellent catalyst for a variety of important reactions, including direct oxidation of hydrocarbon fuels in solid oxide fuel cells (SOFC) [7–9], NO reduction [10,11] and CO oxidation [12,13]. Previously, several studies indicated that the Cu–O–Ce structures and the particular electronic states of Cu and Ce play an important role in the Cu/CeO_2 based catalysts [14,15]. The presence of both Cu^{2+} and Cu^{1+} species in the catalysts has been found by several research groups [14–18]. In a recent work, Ye et al. [19] suggested that Cu loading on CeO_2 not only provides more conductive paths for electrons, but also connects more effective reaction sites, causing an enhancing catalytic activity of ceria. Using the first-principles calculations, Yang et al. [20] and Branda et al. [21] investigated the properties of Cu adsorbed on the CeO_2(1 1 1) surface, and their results demonstrate the existence of Cu^{1+} on the surface of CeO_2, although the extra electron is found to delocalize on three surface Ce ions which contradicts the common sense.

The Ag/CeO_2 system is less studied compared with the cases of Cu/CeO_2 and Au/CeO_2. Scirè et al. [22] prepared Ag/CeO_2 sample and assumed that its high catalytic activity in the methanol combustion is mainly due to the formation of smaller Ag nanoparticles. The same conclusions have been reported by Beier et al. [23].

* Corresponding author at: Department of Physics, Center for Optoelectronics Materials and Devices, Zhejiang Sci-Tech University, Xiasha College Park, Hangzhou 310018, China. Tel.: +86 571 86843655; fax: +86 571 86843655.
E-mail address: siqishihz@gmail.com (S. Shi).

0378-7753/$ – see front matter © 2011 Elsevier B.V. All rights reserved.
doi:10.1016/j.jpowsour.2011.09.026

They suggested that, the Ag exhibits a similar or even more superior catalytic effect in the presence of CeO_2, compared with Pd and Au catalysts. To examine the reduction processes of oxygen molecules on silver cathode surfaces, Wang et al. [24] investigated the monolayer Ag adsorbed on the CeO_2 surfaces, implying that oxygen molecules prefer being reduced at triple-phase boundary (TPB).

Au/CeO_2 system has also been reported to be a prominent catalyst for the water–gas shift (WGS) reaction used for the production of hydrogen in the chemical industry as well as in fuel cell applications [25–28]. The origin of the excellent performance of the Au/CeO_2 catalysts has been extensively studied from both experimental and theoretical points of view. However, the disagreements appear concerning the electronic state of Au adsorbed on the surface of CeO_2. Fu et al. [29,30] and Škoda et al. [31] suggested that the high catalytic activity of Au/CeO_2 arises from positively charged Au. Using the first-principles calculations, Liu et al. [32] also suggested that the high catalytic activity is mostly caused by Au cations instead of the metallic Au particles. A different conclusion was drawn from the X-ray absorption fine-structure (XAFS) spectroscopy by Wang et al. [33,34], indicating that Au nanoparticles remain neutral. Similarly, Castellani et al. [35] investigated the atomic and electronic structures of the Au atom on ceria, and found that Au for most of the active sites remains essentially neutral. Zhang et al. [36] used density functional theory to investigate the nucleation of small Au clusters (up to Au_{11}), and found the contact layer Au atoms bound with surface O atoms are positively charged, which could have significant implications in catalysis. Recently, Branda et al. [21] suggested that the description of Au adsorption is more method dependent due to the nearly degeneracy between the cationic and neutral solutions.

Although some progresses have been achieved, there are still many uncertainties for the Cu/CeO_2, Ag/CeO_2 as well as Au/CeO_2, such as the valence states of the adsorbed M (M = Cu, Ag, and Au), the energetically favorable adsorption sites and the order on the adsorption energy. Especially, it is a scientifically and technologically important issue to characterize and understand the charge transfer and the subsequent localization of electron on surface Ce ions upon the adsorption. In the present paper, we make an attempt to find out the inherent adsorption mechanism of Cu, Ag, and Au on CeO_2(1 1 1) surface using the first-principles calculations based on the density functional theory (DFT), following our previous studies on the effects of M (M = Mn, Pr, Sn, Zr) doping on the redox thermodynamics of bulk CeO_2 [37]. We have comprehensively investigated the surface structures and electronic states of the adsorbed Cu, Ag, and Au on CeO_2(1 1 1) surface. In particular, to the best of our knowledge, the effect of charge distribution upon the adsorption due to the local structural distortions is firstly proposed to understand the interaction between the supported metal atoms and CeO_2(1 1 1) surface. We also discuss the present disagreements on the valence state of the adsorbed Au atom. Moreover, the effects of the exchange-correlation functionals and lattice parameters on the electronic states of Au/CeO_2(1 1 1) interface are clearly communicated in this paper.

2. Computational details

The calculations are performed using the Vienna *ab initio* simulation package (VASP) in the framework of the projector augmented wave method [38–40]. The Perdew–Burke–Ernzerhof (PBE) functional is used for the exchange correlation [41] unless otherwise specified. Furthermore, in order to account for the strong on-site Coulomb repulsion among the Ce 4f electrons, a Hubbard parameter U is added to the PBE functional employing the rotationally invariant approach formulated by Dudarev et al. [42], in which only

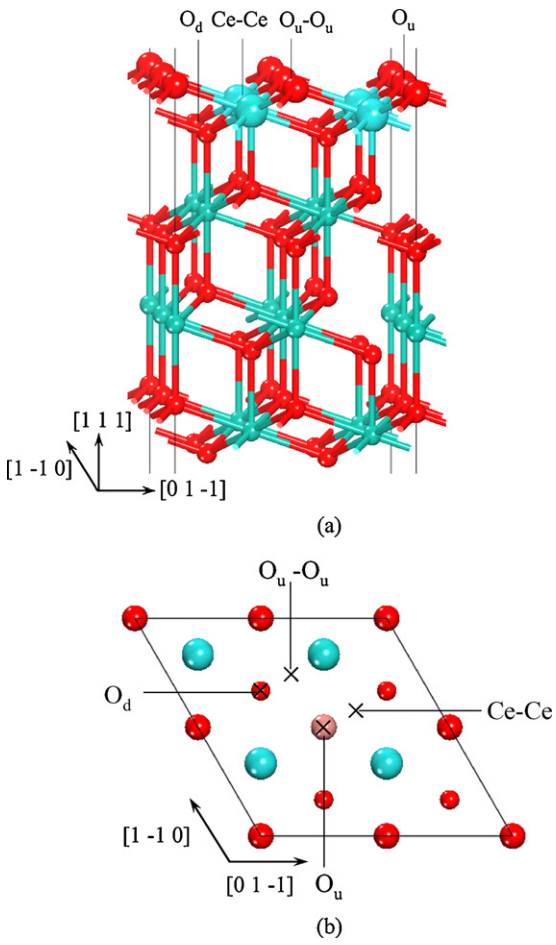

Fig. 1. Possible adsorption sites for M (M = Cu, Ag, Au) on the (2×2) CeO_2(1 1 1) surface: (a) side and (b) top views. Red and blue spheres represent O and Ce atoms, respectively. (For interpretation of the references to color in this figure legend, the reader is referred to the web version of the article.)

the difference ($U_{eff} = U - J$) between the Coulomb U and exchange J parameters enters. Here, we choose a U_{eff} value (hereafter referred to simply as U) with the value of 4.5 eV as suggested by Fabris et al. [43]. The value removes the self-interaction error and thus improves the description of the correlation effects. In particular, the density functional theory (DFT) method has been shown suitable to describe the CeO_2 [44–47].

In our calculations the configurations of Ce $5s^2 5p^6 6s^2 5d^1 4f^1$, O $2s^2 2p^4$, Cu $3d^{10} 4s^1$, Ag $4d^{10} 5s^1$, and Au $5d^{10} 6s^1$ are treated as the valence electrons. We use a plane-wave cutoff energy of 400 eV and $2 \times 2 \times 1$ Monkhorst–Pack k-point mesh [48] with Gaussian smearing of 0.20 eV [49] for the structural optimization and total energy calculations. Total energies are converged to 10^{-7} eV unit cell^{-1}. The Hellmann–Feynman forces are converged to be less than 0.005 eV Å^{-1}. For a more accurate calculation of the electronic density of states (DOS), we apply $4 \times 4 \times 1$ k-point mesh and the modified tetrahedron method [50].

The stoichiometric (1 1 1) surface is modeled by a $p(2 \times 2)$ unit cell with twelve atomic layers and a vacuum layer of 15 Å is introduced to separate the slabs along the z direction. The x and y dimensions of the supercells are fixed at the calculated bulk values, but the ions herein are allowed to relax. The present PBE + U calculations give an equilibrium lattice parameter of 5.49 Å, which is close to the experimental value of 5.41 Å [51]. To model the M/CeO_2 systems, the M atom is put at various active sites on one side of CeO_2 $p(2 \times 2)$ surfaces as depicted below. The bottom six layers are fixed at their bulk positions to mimic the bulk and remaining layers are

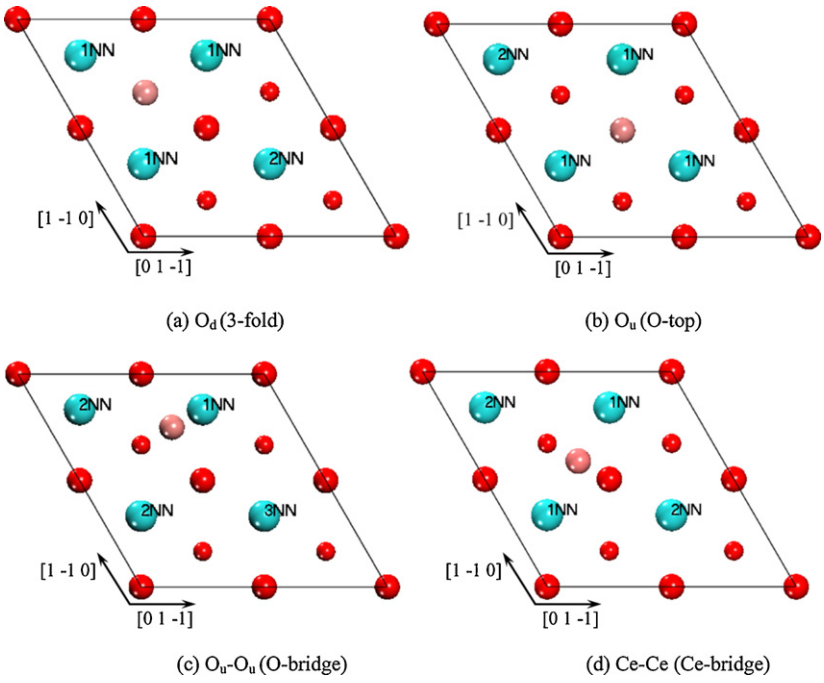

Fig. 2. Structural models of *M* (*M* = Cu, Ag, Au) adsorbed on (a) O_d (3-fold), (b) O_u (O-top), (c) O_u–O_u (O-bridge) and (d) Ce–Ce (Ce-bridge) sites. Red, blue and purple spheres represent O, Ce and *M* atoms, respectively. The notations of 1NN to 3NN indicate the Ce atoms which are the first, second and third nearest neighbors to the adsorbed *M* atom, respectively. (For interpretation of the references to color in this figure legend, the reader is referred to the web version of the article.)

allowed to relax. Prior to VASP optimization, small structural distortions are introduced into the as-built models to achieve various localized solutions. These require slight adjustments of distances between a Ce^{4+} ion cores and nearest-neighboring O ion cores to be consistent with those of a Ce^{3+} ion. The adsorption energy of atom *M* on the CeO_2 surface is calculated by

$$E_{ads} = E_{CeO_2} + E_M - E_{M/CeO_2},$$

where E_{CeO_2}, E_M and E_{M/CeO_2} correspond to the calculated total energies of the clean CeO_2 surface, adsorbed metal atom *M* and combined M/CeO_2 system, respectively.

3. Results and discussion

To explore the various possible adsorption models of *M* (*M* = Cu, Ag, Au) on the CeO_2(1 1 1) surface, the single *M* (*M* = Cu, Ag, Au) atom is placed on the different positions derived from the fold structure of the surface O atom and subsurface Ce atom as shown in Fig. 1, including a three-fold subsurface O-top (O_d) site, a surface O-top (O_u) site, a surface O-bridge (O_u–O_u) site, and a subsurface Ce-bridge (Ce–Ce).

Associated with the adsorption of *M* (*M* = Cu, Ag, Au) atom, a charge transfer between *M* and CeO_2(1 1 1) surface has been clearly observed, causing the appearance of well characterized Ce^{3+} and M^+ cations. It should be noted that, one can find various configurations for 4f electrons to locate at different neighboring Ce ions to the *M* (*M* = Cu, Ag, Au) atom, even for the same adsorption site. As an example, for the three-fold O_d site as shown in Fig. 2a, in the outmost cerium plane, one can find three nearest equivalent Ce cations (1NN) and one second nearest Ce cations (2NN) around the adsorbed metal atom. We find that the electron can actually localize on the outmost surface Ce ion at the 1NN or 2NN to the metal atom with the similar adsorption energies. The same case applies for the one-fold O_u site and Ce–Ce bridge site, i.e., there are also two kinds of charge transfer configurations [see Fig. 2b and d]. However, for the two-fold O_u–O_u site, there are one 1NN Ce ion, two 2NN Ce ions and one 3NN Ce ion around the metal atom, therefore, the electron can localize on the 1NN, 2NN or 3NN Ce ion [see Fig. 2c].

3.1. Cu/CeO_2(1 1 1)

Based on the configurations proposed above, we calculate isosurfaces of excess spin density for Cu adsorbed on CeO_2(1 1 1) surface as shown in Fig. 3. It is interesting to see that, depending on the local atomic configurations, the electron transferred from the Cu atom can localize on the 1NN, 2NN or 3NN Ce ion to the Cu. Table 1 summarizes the adsorption energies, geometries and electronic properties of all the possible adsorption modes of Cu adsorbed on CeO_2(1 1 1) surface. It can be clearly seen that all the considered adsorptions involve the reduction of one of the surface cerium atoms, as indicated by magnetic moments between 0.82 and 0.96 μ_B, which are close to the ideal localized magnetic moment of 1 μ_B per Ce^{3+}. Furthermore, the local environments of the Ce atoms differ from each other due to the larger size of the Ce^{3+} ion compared with the Ce^{4+} ion. The average bond lengths between the localized Ce^{3+} ion and the neighboring O ions for the respective configurations are in the range of 2.45–2.54 Å, which are larger than the theoretical average bond length (2.38 Å) of Ce^{4+}–O, but are comparable to the experimental Ce^{3+}–O bond length of 2.50 Å [52]. Also, this is in reasonable agreement with the average bond length (2.47 Å) of Ce^{3+}–O on the O-deficient CeO_2(1 1 1) surface [52]. Actually, the average bond lengths of Ce^{4+}–O for various configurations are identical to each others. The bond lengths between Cu and surface O atoms are in the range of 1.73–2.07 Å with the value of 2.03 Å for the most stable configuration, which is consistent with the experimental value of 1.86 Å in cubic Cu_2O [53]. It should be mentioned, when the adsorption occurs at the O_u–O_u site, the adsorption energies obey the sequence: 3NN (conf. 1) > 2NN (conf. 2) > 1NN (conf. 3). For the O_d and O_u sites, the adsorption at the 2NN (conf. 1) site is also more energetically favorable than that at the 1NN (conf. 2) site. Therefore, we may assume that for the same adsorption site, the excess electrons localize preferentially at the Ce ion relatively far way from the adsorbed Cu. Note that, the systems

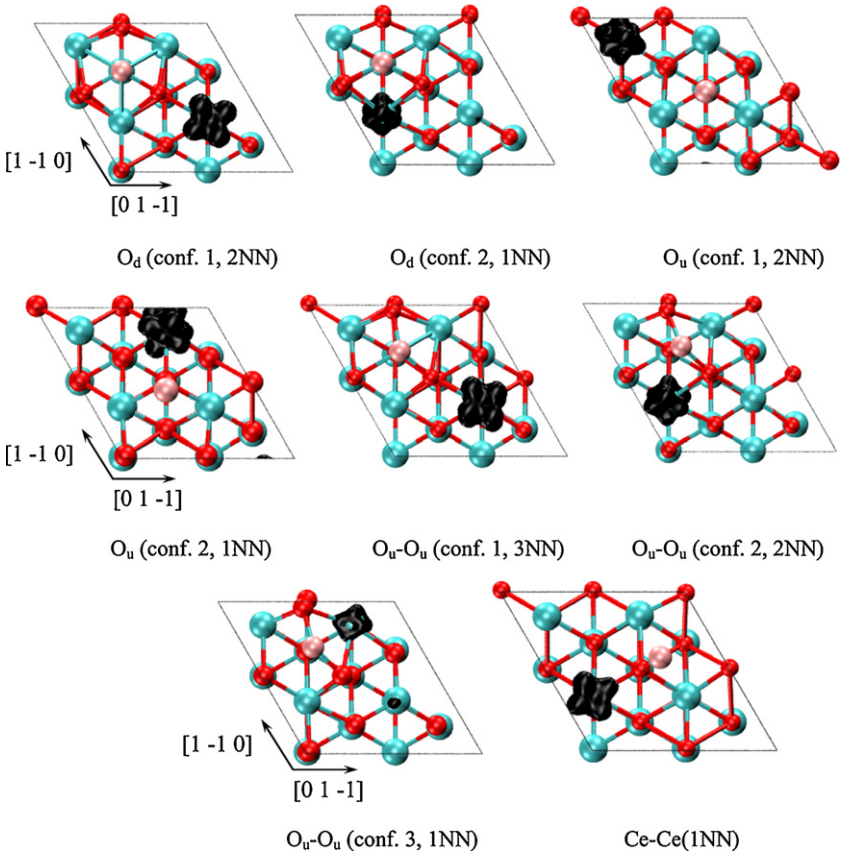

Fig. 3. Isosurfaces of excess spin charge density for Cu adsorbed on different sites of CeO_2(1 1 1) surface. The labeling corresponds to the description of configuration and the location of the Ce^{3+} ion in Table 1 and Fig. 2.

have to be distorted slightly beforehand to obtain these configurations, causing the atomic environment of the desired initial position Ce^{4+} ions, to a large extent, to be consistent with that of the Ce^{3+}. To our knowledge, the phenomenon that the slight structural distortion can cause the complete oxidization of adsorbed metal atom *M* in *M*/CeO_2 interfaces has never been reported in the literatures, although similar one has been observed from the investigations of the O-vacancy on the CeO_2(1 1 1) surface by Ganduglia-Pirovano et al. [52] and Li et al. [54], which indicated that there exist multiple configurations of the two excess electrons localization associated with the formation of an O-vacancy on the CeO_2(1 1 1) surface.

From our calculations, the Cu adsorption at the three-fold O_d site is the most energetically favorable with the adsorption energy of 2.62 eV, which is consistent with the results of Branda et al. [21] and Yang et al. [20]. However, it should be emphasized that all calculations on the Cu adsorption at the O_d, O_u–O_u and O_u sites by Branda et al. [21] and Yang et al. [20] indicate that electron released from neutral metal atom delocalizes on all three nearest neighboring (NN) Ce ions, which is different from our conclusion, i.e., the transferred charge should localize on one 2NN Ce ion with the magnetic moment of 0.96 μ_B. In fact, the electron transfer from Cu to a *single* Ce ion can be applied for all the configurations in our work. We also find the delocalized structures obtained are less stable than the localized ones and the corresponding Ce^{4+} is not completely reduced to Ce^{3+}. Therefore, we argue that the localized solution is more reasonable. A similar conclusion has also been drawn from our previous investigation on the O-vacancy in bulk CeO_2, in which the two excess electrons upon the formation of the O-vacancy prefer localizing on two NN Ce ions instead of delocalizing on four NN Ce ions [37].

Since the adsorption is accompanied by a charge transfer from Cu to an unoccupied Ce 4f level, it is significant to understand the electronic properties of the adatom Cu and substrate atoms. Here we take the most energetically favorable O_d (conf.1) model for an example and analyze the respective partial density of states (PDOS) of Cu atom, pure CeO_2(1 1 1), and Cu/CeO_2(1 1 1) as shown

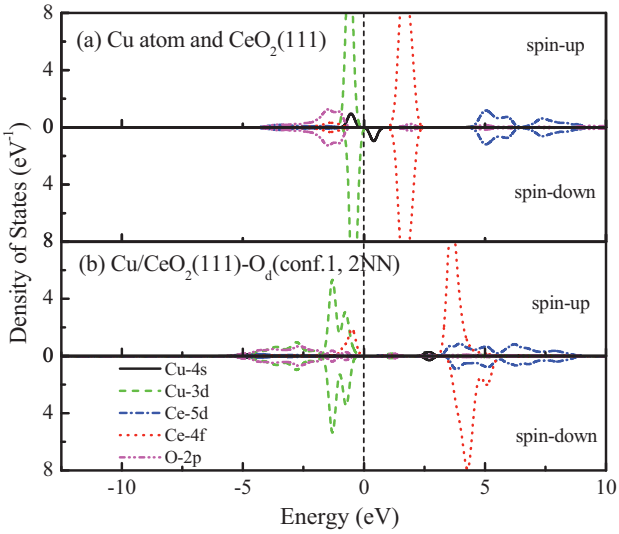

Fig. 4. Partial density of states (PDOS) of Cu atom, pure CeO_2(1 1 1) and Cu adsorbed on O_d site (conf-1, 2NN). The zero point of the energy axis corresponds to the Fermi level, whereas the upper and lower panels represent the spin up and spin down channels, respectively.

Table 1
Adsorption energies, geometries and electronic properties for the adsorption configurations of Cu/CeO_2(1 1 1). $d_{(Cu-O)}$ and $d_{(Cu-Ce)}$ are distances from the adsorbed Cu to surface O and Ce atoms, respectively. μ_{Ce} and μ_{Cu} are the magnetic moments of reduced Ce (in bold) and oxidized Cu, respectively. $d_{(Ce-O)}$ corresponds to the average Ce^{3+}–O bond length. Previous results are also listed for comparison.

Site	E_{ads} (eV)	$d_{(Cu-O)}$ (Å)	$d_{(Cu-Ce)}$ (Å)	μ_{Ce} (μ_B)	μ_{Cu} (μ_B)	$d_{(Ce-O)}$ (Å)	Reference
			3×2.88	0.00			
O_d (conf.1, 2NN)	2.62	3×2.03	1×4.75	**0.96**	0.00	2.54	Present work
		1×2.04	2×2.87	0.01			
	2.10	2×2.07	1×2.89	**0.86**	0.00	2.46	Present work
			1×4.83	0.10			
O_d (conf.2, 1NN)		1×2.01	2×2.78	0.16, 0.19			[21]
	1.86	2×2.04	1×2.79	0.34	0.00		VASP-(L5)L5//G3[a]
	2.68	1×2.03	1×2.88				[20]
			2×3.70	0.00			
O_u (conf.1, 2NN)	1.71	1×1.77	1×3.81	0.00	0.01	2.48	Present work
			1×5.22	**0.89**			
			2×3.60	0.00			
	1.63	1×1.78	1×3.88	**0.91**	0.02	2.46	Present work
			1×4.95	0.00			
O_u (conf.2, 1NN)			1×3.57	0.18			[21]
	1.50	1×1.73	1×3.61	0.16	0.08		VASP-(L5)L5//G3[a]
			1×3.65	0.22			
	1.63						[20]
			1×2.77	0.00			
O_u–O_u (conf.1, 3NN)	2.45	2×1.94	2×3.02	0.00	0.00	2.52	Present work
			1×4.66	**0.96**			
			1×2.70	0.00			
O_u–O_u (conf.2, 2NN)	2.17	1×1.90	1×3.19	**0.94**	0.00	2.48	Present work
		1×1.93	1×3.30	0.00			
			1×4.51	0.00			
			1×2.77	**0.90**			
O_u–O_u (conf.3, 1NN)	2.06	2×1.93	2×3.07	0.00	0.00	2.51	Present work
			1×4.79	0.00			
			1×2.61	0.28	0.00		[21]
	1.61	2×1.89	2×3.13	0.30, 0.45			VASP-(L5)L5//G3[a]
			2×3.35	0.02			
Ce–Ce	1.44	1×1.80	1×4.17	**0.86**	0.03	2.45	Present work
			1×5.72	0.00			

[a] The notation of (L5)L5//G3 indicates that lattice parameter and geometry optimization are carried out at the LDA + U (U = 5 eV) level whereas the energy and electronic properties arise from single point calculations at the GGA + U (U = 3 eV) level.

in Fig. 4. It can be seen from Fig. 4a that for the Cu atom, there is an asymmetric occupied peak corresponding to the Cu 4s state. However, the adsorption of Cu at the CeO_2(1 1 1) surface obviously gives rise to the disappearance of the occupied Cu 4s gap state as shown in Fig. 4b, indicating that the single Cu 4s electron has been released in Cu/CeO_2 system. Moreover, there is a new occupied peak corresponding to the Ce 4f states for the Cu/CeO_2(1 1 1), further confirming that the electron indeed localizes on the 2NN Ce ion, thus making Ce^{4+} and Cu reduced and oxidized to Ce^{3+} and Cu^+, respectively. This is in good agreement with the previous experimental results, which indicate that the adsorbed Cu on CeO_2(1 1 1) surface would be oxidized to Cu^+ [14,55,56], which is also consistent with suggestion of Hornés et al. [57] that a high catalytic activity of CO oxidation of CeO_2/CuO system are related to interfacial Cu^+ species generated during the reaction.

3.2. Ag/CeO_2(1 1 1)

Following the same methodology, we extend our studies to the Ag/CeO_2(1 1 1) system, as shown in Table 2. We also find the adsorption on the three-fold O_d site is the most energetically favorable and correspondingly, the single electron transfers from the adsorbed Ag neutral atom to the 2NN Ce^{4+} cation although there are some variances from Cu/CeO_2(1 1 1). Note that, both O_u–O_u and Ce–Ce models in Ag/CeO_2 system are unstable and converged to the O_d one upon the structural optimization. This is in a good agreement with the results of Branda et al. [21]. Therefore, it can be concluded that only O_d and O_u adsorption configurations exist for the Ag/CeO_2(1 1 1) system by using the density functional theory study.

It is also found from Table 2 that the transferred electron for all the calculated models localizes on a single Ce ion. Similar to the case of Cu/CeO_2(1 1 1) system, there exist the different Ce 4f electron localization configurations for the O_d and O_u adsorption sites, and the electron preferentially localizes on the surface Ce ion which is relatively far away from the adsorbed Ag, which from results in Ref. [21]

Magnetic moments of the localized Ce ions for all the configurations are in the range of 0.80–0.96 μ_B, which are close to 1 μ_B/Ce^{3+}. Moreover, the calculated average bond lengths of Ag^+–O in respective configurations are in the range of 2.01–2.47 Å with three Ag^+–O bond lengths of 2.36, 2.36 and 2.38 Å for the most stable configuration, which are slightly larger than the experimental value of 2.05 Å in cubic Ag_2O [58]. This can be understood from the fact that three and two-fold Ag–O bonds occur in the Ag/CeO_2(1 1 1) (O_d adsorption configuration) and cubic Ag_2O, respectively. These analyses demonstrate that Ag atom is indeed oxidized to Ag^+. This is consistent with the result presented by Branda et al. [21], although they did not observe the multiple configurations with the excess electron localized at different neighboring Ce ions. The similar conclusion has been drawn by Wang et al. [24], who investigated a CeO_2(1 1 1) supported atomic layer of silver using a (2×2) slab model with four Ag atoms. Results indicated that there is 0.14 electron on the adsorbed monolayer Ag, which reveals that all four Ag atoms are nearly oxidized to Ag^+. Experimentally, Farmer et al. [59] studied the Ag adsorption on reduced CeO_2(1 1 1) thin films using

Table 2
Adsorption energies, geometries and electronic properties for the adsorption configurations of Ag/CeO_2(1 1 1). $d_{(Ag-O)}$ and $d_{(Ag-Ce)}$ are distances from the adsorbed Ag to surface O and Ce atoms, respectively. μ_{Ce} and μ_{Ag} are the magnetic moments of reduced Ce (in bold) and oxidized Ag, respectively. $d_{(Ce-O)}$ corresponds to the average Ce^{3+}–O bond length. Previous results are also listed for comparison.

Site	E_{ads} (eV)	$d_{(Ag-O)}$ (Å)	$d_{(Ag-Ce)}$ (Å)	μ_{Ce} (μ_B)	μ_{Ag} (μ_B)	$d_{(Ce-O)}$ (Å)	Reference
		2×2.36	1×3.18	0.01			
O_d (conf.2, 2NN)	1.42	1×2.38	2×3.19	0.00	0.00	2.50	Present work
			1×4.94	**0.96**			
		2×2.47	1×3.17	**0.90**			
O_d (conf.1, 1NN)	1.11	1×2.34	2×3.15	0.00	0.00	2.47	Present work
			1×4.98	0.01			
	1.00	3×2.28	3×3.07	0.89	0.00		[21]
			2×3.86	0.01			
O_u (conf.1, 2NN)	0.86	1×2.07	1×4.00	0.00	0.02	2.47	Present work
			1×5.31	**0.82**			
			2×3.76	0.00			
	0.83	1×2.08	1×4.11	**0.80**	0.03	2.45	Present work
			1×5.02	0.00			
O_u (conf.2, 1NN)			1×3.65				
	0.56	1×2.01	1×3.75	**0.64**	0.07		[21]
			1×3.81				

adsorption microcalorimetry and found that the heat of adsorption of Ag vapor is 2.07 eV (200 kJ mol^{-1}), which is much larger than the present value of 1.42 eV. This may be attributed to the existence of O-vacancies on reduced CeO_2(1 1 1).

3.3. Au/CeO_2(1 1 1)

In spite of much attention paid on Au/CeO_2 system, both the oxidizations states of the adatom Au and energetically favorable adsorption configuration are still pending issues. The present PBE + *U* calculations indicate that Au located at the bridge-site has the largest adsorption energy which is consistent with the one by Hernández et al. [60] and Camellone et al. [61], Zhang et al. [62] and Branda et al. [21] However, Liu et al. [32], Castellani et al. [35] and Chen et al. [63] stated that Au adsorption at the O-top of the CeO_2(1 1 1) surface is the most stable. The disagreement lies in the choice of the ultrasoft pseudopotentials, the value of the *U* or cut-off energy used to describe the valence electrons [21,35]. Table 3 summarizes the adsorption energies, relevant bond lengths and magnetic moments for a single Au atom on the CeO_2(1 1 1) surface together with the theoretical and experimental results reported in the literatures [21,60–63]. The most stable adsorption configuration is the O_u–O_u model with the electron localized on the 3NN Ce ion to the Au. The adsorption energy and Au–O bond length in the present work are 0.99 eV and 2.15 Å, respectively, which are very close to those (1.15 eV and 2.15 Å) of Hernández et al. [60] using the GGA + *U* formulation with the *U* value of 5.0 eV.

Accordingly, it can be seen from Table 3 that there are also different configurations with the excess electron localized on the different Ce ions. In other words, similar to the cases of the Cu/CeO_2(1 1 1) and Ag/CeO_2(1 1 1) systems, the excess electron derived from the Au adsorption at the O_u, O_d and O_u–O_u sites can condense into the localized 4f-level traps of the 1NN, 2NN or 3NN Ce ion. Moreover, for the same adsorption site, the longer the distance between the surface Ce ion with localized electron and the adsorbed Au atom is, the more energetically favorable the configuration becomes.

Moreover, Zhang et al. [62] suggested that there is a distribution of Au^0 (hollow site) or Au^+ (top and bridge site) atomic species at the regular sites of the CeO_2(1 1 1) surface and Baron et al. [64] believed that there exists partially charged $Au^{\delta+}$ on CeO_2(1 1 1). Recently, Branda et al. [21,65] argued that the description of Au/CeO_2(1 1 1) is more method dependent and there exist two well-defined states with similar energy but exhibit different electronic structures and local geometries, i.e., one with fully oxidized Au and the other with neutral Au. However, our calculations indicate that, independent of the location of Au at the surface site, the adsorption of Au atom on CeO_2(1 1 1) surface is always accompanied by the one-electron charge transfer from Au atom to a neighboring Ce ions, which is independent on the adsorption sites. As an example shown in Table 3, in the case of adsorption on the O_u–O_u site with the electrons transferred to the 3NN Ce ion, the magnetic moment of Ce^{3+} is 0.97 μ_B and the Au atom is oxidized to Au^+ ion.

To further analyze the interaction between the adsorbed Au atom and CeO_2(1 1 1) surface, we examine the degree of the charge transfer between Au and the CeO_2(1 1 1) surface. Bader charge based analysis [66] predicts that the adsorbed Au loses about 1.3e, revealing a completely oxidization process. The analysis of PDOS for Au/CeO_2(1 1 1) provides a further confirmation. It can see seen from Fig. 5 that its 6s state upon the Au atom adsorption becomes unoccupied and a new peak emerges between O 2p valance band top and unoccupied Ce 4f band bottom. In other words, the adsorbed Au is oxidized whereas the 3NN Ce^{4+} is reduced to Ce^{3+}. Actually, one can observe always a single neighboring completely reduced Ce ion for all the considered adsorption configurations. Experimental results also support the present conclusion. For example, Fu et al. [30] found Au^+ by using the X-ray photoelectron spectroscopy (XPS)

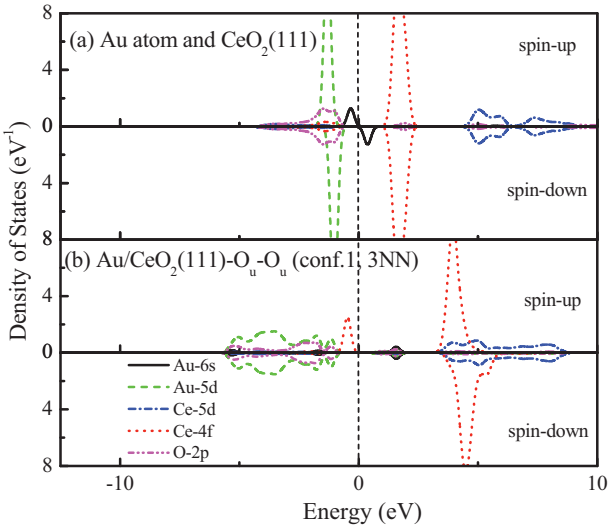

Fig. 5. Partial density of states (PDOS) of Au atom, pure CeO_2(1 1 1) and Au adsorbed on O_u–O_u site (conf-1, 3NN). The zero point of the energy axis corresponds to the Fermi level, whereas the upper and lower panels represent the spin up and spin down channels, respectively.

Table 3
Adsorption energies, geometries and electronic properties for the adsorption configurations of Au/CeO_2(1 1 1). $d_{(Au-O)}$ and $d_{(Au-Ce)}$ are distances from the adsorbed Au to surface O and Ce atoms, respectively. μ_{Ce} and μ_{Au} are the magnetic moments of reduced Ce (in bold) and oxidized Au, respectively. $d_{(Ce-O)}$ corresponds to the average Ce^{3+}–O bond length. Previous results are also listed for comparison.

Site	E_{ads} (eV)	$d_{(Au-O)}$ (Å)	$d_{(Au-Ce)}$ (Å)	μ_{Ce} (μ_B)	μ_{Au} (μ_B)	$d_{(Ce-O)}$ (Å)	Reference
		2×2.35	1×3.11	0.01			
O_d (conf.1, 2NN)	0.69	1×2.36	2×3.12	0.00	0.02	2.49	Present work
			1×4.89	**0.91**			
		1×2.22	2×3.15	0.01			
	0.67	2×2.62	1×3.19	**0.84**	0.02	2.47	Present work
			1×4.98	0.00			
	0.61	3×2.76	3×3.27	0.10			
O_d (conf.1, 1NN)			1×5.06	0.02			[60]
		1×2.56	1×3.05				
	0.51	1×2.58	1×3.08	0.14	0.25		[21]
		1×2.63	1×3.10				
	0.66						[62]
			2×3.80	0.01			
	0.90	1×2.00	1×3.95	0.01	0.08	2.46	Present work
			1×5.26	**0.77**			
			2×3.85	0.00			[60]
	0.96	1×1.96	1×3.93	0.00			
			1×5.32	**0.96**			
	0.66	1×2.07	2×3.62	<0.1	0.31		[21]
			1×3.63				
O_u (conf.1, 2NN)	1.26						[32]
	1.04	1×2.00					[61]
	0.96						[62]
	0.78	1×2.18					[63] SIESTA-PBE
	0.63	1×2.18					[63] SIESTA-BLYP
	0.88	1×2.23					[63] VASP
			1×3.69	0.00			
			1×3.70	0.00			
	0.85	1×2.02	1×4.03	**0.62**	0.15	2.42	Present work
O_u (conf.2, 1NN)			1×5.01	0.00			
			2×3.50	0.00			
	0.92	2.06	1×4.22	**0.83**			[60]
			1×4.60	0.00			
			1×2.85	0.00			
	0.99	2×2.15	2×2.31	0.00	0.00	2.49	Present work
			1×4.62	**0.97**			
			1×2.85	0.00			
O_u–O_u (conf.1, 3NN)	1.15	2×2.15	2×2.32	0.00			[60]
			1×4.63	**0.97**			
	1.18		1×4.76				[61]
	1.04		1×2.85				[62]
			2×3.35				
		1×2.14	1×2.83	0.00			
	0.86	1×2.21	2×3.38	**0.95**	0.00	2.49	Present work
			1×4.67	0.00			
O_u–O_u (conf.2, 2NN)		1×2.15	1×2.83	0.00			
	1.00	1×2.21	1×3.37	**0.96**			[60]
			1×3.40	0.00			
			1×4.66	0.00			
	1.25		1×3.34				
			1×2.87	**0.91**			
	0.70	2×2.20	2×3.29	0.01	0.00	2.47	Present work
			1×4.76	0.03			
O_u–O_u (conf.3, 1NN)			1×2.87	**0.95**			
	0.86	2×2.21	2×3.30	0.00			[60]
			1×4.75	0.00			
	0.43	2×2.15	1×2.76	2×0.47	0.00		[21]
			2×3.25				
			2×3.63	0.00			
Ce–Ce	0.85	1×2.03	1×4.13	**0.68**	0.00	2.43	Present work
			1×5.67	0.00			

technique. They also suggested the catalytic activity was affected by the ionic state Au instead of metallic Au.

In the following we will focus on the effects of exchange-correlation functional and lattice parameters on the oxidization states of Au. Here, following the calculation procedures in the present work, we examine the oxidization states of Au for the top O_u site model using both GGA + U (U = 5.0) and LDA + U (U = 5.0) with both cell parameters a_0 = 5.40 and 5.49 Å so as to make the overall comparison with the results of Branda et al. [65], as shown in Table 4. Both GGA + U (U = 5.0) and LDA + U (U = 5.0) calculations for the case of a_0 = 5.49 Å inevitably lead to the same conclusions. That is, the adatom Au is almost oxidized and one surface Ce^{4+}

Table 4
Adsorption energies, geometries and electronic properties for the adsorption configurations of Au/CeO_2(1 1 1) using GGA + U and LDA + U methods. $d_{(Au-O)}$ and $d_{(Au-Ce)}$ are distances from the adsorbed Au to surface O and Ce atoms, respectively. μ_{Ce} and μ_{Au} are the magnetic moments of reduced Ce (in bold) and oxidized Au, respectively. $d_{(Ce-O)}$ corresponds to the average Ce^{3+}–O bond length. Previous results are also listed for comparison.

Site	E_{ads} (eV)	$d_{(Au-O)}$ (Å)	$d_{(Au-Ce)}$ (Å)	μ_{Ce} (μ_B)	μ_{Au} (μ_B)	$d_{(Ce-O)}$ (Å)	Reference
GGA + U (a_0 = 5.49, U = 5.0)							
			1 × 3.81	0.00			
			1 × 3.82	0.00			
Conf. 1 (2NN)	1.09	1 × 1.98			0.02	2.48	Present work
			1 × 3.95	0.01			
			1 × 5.27	**0.87**			
			1 × 3.78	0.00			
			1 × 3.79	0.00			
Conf. 2 (1NN)	0.99	1 × 1.99	1 × 3.95	**0.82**	0.06	2.45	Present work
			1 × 5.18	0.00			
LDA + U (a_0 = 5.49, U = 5.0)							
			2 × 3.68	0.00			
Conf. 1 (2NN)	1.57	1 × 1.94	1 × 3.84	0.00	0.03	2.44	Present work
			1 × 5.18	**0.78**			
			2 × 3.56	0.00			
Conf. 2 (1NN)	1.51	1 × 1.96	1 × 3.93	**0.57**	0.09	2.40	Present work
			1 × 4.90	0.00			
GGA + U (a_0 = 5.49, U = 5.0)	0.96			0.94[a]	0.07		[65]
LDA + U (a_0 = 5.49, U = 5.0)	1.37			0.93[a]	0.07		[65]
GGA + U (a_0 = 5.40, U = 5.0)							
			1 × 3.81	0.01			
Conf. 1 (2NN)	0.91	1 × 1.99	1 × 3.82	0.01	0.06	2.45	Present work
			1 × 3.93	0.01			
			1 × 5.23	**0.81**			
			1 × 3.67	0.00			
Conf. 2 (1NN)	0.80	1 × 2.03	1 × 3.68	0.00	0.12	2.41	Present work
			1 × 4.06	**0.68**			
			1 × 4.92	0.01			
LDA + U (a_0 = 5.40, U = 5.0)							
			2 × 3.66	0.01			
Conf. 1 (2NN)	1.54	1 × 1.96	1 × 3.82	0.01	0.10	2.40	Present work
			1 × 5.12	**0.70**			
			2 × 3.53	0.01			
Conf. 2 (1NN)	1.50	1 × 1.99	1 × 3.91	**0.53**	0.19	2.36	Present work
			1 × 4.86	0.01			
GGA + U (a_0 = 5.40,U = 5.0)	0.61			0.06–0.10[b]	0.33		[65]
LDA + U (a_0 = 5.40, U = 5.0)	1.27			0.07–0.10[b]	0.32		[65]

[a] Fully localized on one Ce atom, 2NN to the O–Au bond.
[b] Delocalized over four Ce atoms.

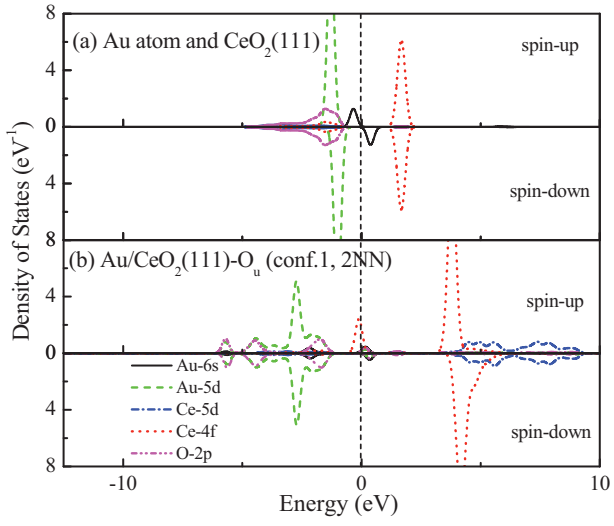

Fig. 6. Partial density of states (PDOS) of Au atom, pure CeO_2(1 1 1) and Au adsorbed on O_u site (conf-1, 2NN). The calculation are performed with GGA + U (U = 5.0), a_0 = 5.40 Å. The zero point of the energy axis corresponds to the Fermi level, whereas the upper and lower panels represent the spin up and spin down channels, respectively.

ion is reduced, which is in good agreement with the conclusion in Ref. [65]. As for the case of a_0 = 5.40 Å, the magnetic moments of Ce ion using both GGA + U (U = 5.0) and LDA + U (U = 5.0) calculations are found to be 0.53–0.81 μ_B, indicating Au is also oxidized. This disagrees with the suggestion of Branda et al. [65], in which the magnetic moment of Ce ion around the adatom Au is small ($\mu_{Ce} \leq 0.1\ \mu_B$). We notice that Branda et al. [65] did not supply the electronic structure analysis. In order to further reveal the oxidized state of the adatom Au and make comparison with the PBE + U calculations, we analyze the PDOS for GGA + U (U = 5.0), a_0 = 5.40 Å with electrons localized on the 2NN Ce ions, as shown in Fig. 6. We can see that the adsorption of Au atom causes the occurrence of a new occupied peak corresponding to localized Ce 4f states [see Fig. 6b]. Meanwhile, the occupied Au 6s states in Fig. 6a are shifted above the Fermi level, indicating that Au indeed loses electron. This is in good agreement with the result of PDOS using PBE + U method. Therefore, we believe that, structural distortion instead of the reasonable choice of exchange-correlation functional and lattice parameters as previously suggested [65], is more important to achieve the oxidization of Au and a localized solution. Tests are performed for Cu/CeO_2(1 1 1) and Ag/CeO_2(1 1 1) systems by varying exchange-correlation functional and lattice parameters and reveal no dependence of our conclusions on the choice of adsorption species. In addition, both Branda et al. [65] and we report that adsorption energies using LDA + U calculations are larger than those

using GGA + U and PBE + U ones which is largely because the LDA somewhat overestimates surface energies [67].

4. Discussion

Based on the above results, we can conclude in the cases of M (M = Cu, Ag, Au) adsorbed on CeO_2(1 1 1) surface, Cu and Ag prefer to be adsorbed on the O_d site, whereas Au is at the O_u–O_u site. We notice that Yang et al. [68,69], who studied Pd and Pt adsorbed on CeO_2(1 1 1), found that Pd and Pt prefer to be adsorbed on the O-bridge (O_u–O_u) and 3-fold O_d sites, respectively. However, the electron is found to be delocalized around the adsorption site and adatoms Pd and Pt are only partially oxidized. Recently Bruix et al. [70] predicted that the most favorable interaction for the Pt/CeO_2(1 1 1) corresponds to adsorption on top of a site bridging two nearest-neighbor surface O atoms in a closed-shell electronic configuration with an essentially neutral or slightly positively charged Pt. Nevertheless, for this site another slightly higher energy solution is found with two unpaired electrons in the unit cell and the adsorption represents a completely different physical picture, where the adatom Pt has been oxidized to Pt^+ with the concomitant reduction of a single Ce^{4+} to Ce^{3+}. Besides, Chafi et al. [71] investigated the Ni–CeO_2 interaction using the GGA scheme and found that the O_u top site is the most stable. We can say that the electronic states of Pt (Pd, Ni)/CeO_2 systems mentioned above are somewhat contentious, which should be reasonably characterized via analysis of the local structural distortions. In other words, for the purpose of achieving the energetically stable structures, the interaction of metal adatom with stoichiometric CeO_2(1 1 1) surface will result in the complete oxidization of the adatom and the formation of adatom–O–Ce bonds. The present results are supported by previous experimental investigations. For example, Fu et al. [30] suggested that there are stable Au–O–Ce structures in Au/CeO_2. Using the X-ray diffraction (XRD) and X-ray absorption fine-structure (XAFS) techniques, similar argument can be made for the Cu–CeO_2, Pt–CeO_2 and Pd–CeO_2, in which the M–O–Ce bonds are formed [14,15,72].

We find that the order on the adsorption energy of metal (Cu, Ag, Au) on CeO_2(1 1 1) follows the Cu > Ag > Au. This is consistent with the conclusion in Ref. [21]. Our further analysis of electronic structures indicates that the excess electron upon the M (M = Cu, Ag, Au) adsorption can indeed localize on the different Ce ions. For the same adsorption site, a general rule is that the electron prefers to localize on Ce ion which is far from the adsorbed M (M = Cu, Ag, Au). However, there are some differences among Cu, Ag, and Au adsorption. For the case of Ag adsorbed, the O_u–O_u and Ce–Ce site can spontaneously converge to O_u site.

It must be emphasized that most of configurations with the excess electrons localized at different neighboring Ce ions cannot be derived from direct relaxation from the ideal CeO_2(1 1 1) surface. For example, for the undistorted structures of Cu and Ag adsorbed on O_u site, the excess electron delocalizes at three NN Ce ions and structures are not stable with the smaller adsorption energies by 0.2–0.35 eV as compared with the distorted cases. Thus, structural distortion is necessary to achieve a desired as well as localized configuration. In other words, the local structural distortion enables the excess electron to be localized at different sites. As compared with the delocalized solutions based on the undistorted structures, the variations of M–O and M–Ce bond lengths caused by the structural distortions are only in the small range of 0.01–0.04 Å and 0.11–0.24 Å, suggesting that experimental realization is feasible by doping or controlling the atmosphere. Recent investigation [73] regarding the effects for Ti, Zr, and Hf doping on CO and NO adsorption on CeO_2(1 1 0) surface has shown that the dopants seek and replicate its most favored coordination environment, leading to a distorted atomic structure of the host oxide. These experimental findings correlate well with our work. The combinations of experimental result with our work deepen the understanding of the catalytic properties of CeO_2 surface supported metal clusters and could also be expanded to other important metal/oxide systems.

The rationalization why there exist the various electron localization configurations can be interpreted by adopting the opinion of Madelung potential as suggested in Ref. [52], which states that the more energetically favorable, the lower Madelung potential. Besides, the possibility of the direct f–f hopping for Ce ions, the geometric structure, and the intrinsic characteristics of 4f electrons have also been suggested to explain the charge distribution in ceria-based catalyst [49,74,75].

5. Conclusion

Adsorption mechanisms of metal (Cu, Ag, and Au) on CeO_2(1 1 1) surface have been investigated using the first-principles density-functional theory calculations considering the on-site Coulomb interaction within the PBE + U scheme. The systematical analysis of the adsorptions energies, atomic and electronic structures reveals that the energetically favorable configuration for Cu and Ag adsorption is at the 3-fold O_d site, whereas one for Au adsorption is at the O_u–O_u site. Cu atom exhibits the largest adsorption energy, followed by Ag and then Au. Adsorption is accompanied by a charge transfer process, which makes the adsorbed metal atom completely oxidized and one of the neighboring Ce^{4+} reduced. Charge redistribution with electron localized on different Ce ions neighboring to adsorbed atom is observed. Adsorption configuration with the excess electron localized on the surface Ce ion away from the adsorbed metal is energetically more favorable. It has also been found the structural distortion play a decisive role for understanding metal atoms adsorbed on CeO_2(1 1 1) surface. The present methodology and observed phenomena are not only significant for theoretical investigations, but also provide a rational guidance for the experimental studies.

Acknowledgments

The present work is supported by National 973 Program of China (2012CB215402), National Natural Science Key Foundation of China (NSFC) (No. 50730004), National Natural Science Foundation of China (NSFC) (Nos. 51072183 and 50802089) and Natural Science Foundation of Zhejiang Province (No. Y4090280).

References

[1] A. Trovarelli, Catalysis by Ceria and Related Materials, Imperial College Press, London, 2002.
[2] A. Trovarelli, C. de Leitenburg, M. Boaro, G. Dolcetti, Catal. Today 50 (1999) 353.
[3] B.C.H. Steele, A. Heinzel, Nature (London) 414 (2001) 345.
[4] X. Liu, K. Zhou, L. Wang, B. Wang, Y. Li, J. Am. Chem. Soc. 131 (2009) 3140.
[5] M. Daturi, N. Bion, J. Saussey, J.C. Lavalley, C. Hedouin, T. Seguelong, G. Blanchard, Phys. Chem. Chem. Phys. 3 (2001) 252.
[6] V. Skorodumova, S.I. Simak, B.I. Lundqvist, I.A. Abrikosov, B. Johansson, Phys. Rev. Lett. 89 (2002) 166601.
[7] S. Park, J.M. Vohs, R.J. Gorte, Nature 404 (2000) 265.
[8] Y.M. Choi, C. Compson, M.C. Lin, M.L. Liu, Chem. Phys. Lett. 421 (2006) 179.
[9] Y.M. Choi, C. Compson, M.C. Lin, M.L. Liu, J. Alloys Compd. 427 (2007) 25.
[10] B. Wen, M. He, Appl. Catal. B 37 (2002) 75.
[11] P. Bera, K.R. Priolkar, P.R. Sarode, M.S. Hegde, S. Emura, R. Kumashiro, N.P. Lalla, Chem. Mater. 14 (2002) 3591.
[12] G.L. Xiao, C.N. Xian, H. Li, L.Q. Chen, J. Nanosci. Nanotechnol. 11 (2011) 1923.
[13] J.B. Park, J. Graciani, J. Evans, D. Stacchiola, S.D. Senanayake, L. Barrio, P. Liu, J.F. Sanz, J. Hrbek, J.A. Rodriguez, J. Am. Chem. Soc. 132 (2010) 356.
[14] D. Gamarra, G. Munuera, A.B. Hungría, M. Fernández-García, J.C. Conesa, P.A. Midgley, X.Q. Wang, J.C. Hanson, J.A. Rodríguez, A. Martínez-Arias, J. Phys. Chem. C 111 (2007) 11026.
[15] R. Kydd, W.Y. Teoh, K. Wong, Y. Wang, J. Scott, Q.-H. Zeng, A. Yu, J. Zou, R. Amal, Adv. Funct. Mater. 19 (2009) 369.

[16] G. Avgouropoulos, T. Ioannides, H. Matralis, Appl. Catal. B 56 (2005) 87.
[17] G. Avgouropoulos, T. Ioannides, Appl. Catal. A 244 (2003) 155.
[18] P. Djinović, J. Batista, A. Pintar, Appl. Catal. A 347 (2008) 23.
[19] X.F. Ye, S.R. Wang, Q. Hu, J.Y. Chen, T.L. Wen, Z.Y. Wen, Solid State Ionics 180 (2009) 276.
[20] Z.X. Yang, B.L. He, Z.S. Lu, K. Hermansson, J. Phys. Chem. C 114 (2010) 4486.
[21] M.M. Branda, N.C. Hernández, J.F. Sanz, F. Illas, J. Phys. Chem. C 114 (2010) 1934.
[22] S. Scirè, C. Crisafulli, S. Giuffrida, C. Mazza, P.M. Riccobene, A. Pistone, G. Ventimiglia, C. Bongiorno, C. Spinella, Appl. Catal. A 367 (2009) 138.
[23] M.J. Beier, T.W. Hansen, J.-D. Grunwaldt, J. Catal. 266 (2009) 320.
[24] J.H. Wang, M.L. Liu, M.C. Lin, Solid States Ionics 177 (2006) 939.
[25] C.W. Sun, H. Li, L.Q. Chen, J. Phys. Chem. Solids 68 (2007) 1785.
[26] W.-J. Zhu, J. Zhang, X.-Q. Gong, G.Z. Lu, Catal. Today 165 (2011) 19.
[27] K. Naya, R. Ishikawa, K. Fukui, J. Phys. Chem. C 113 (2009) 10726.
[28] C.J. Weststrate, R. Westerström, E. Lundgren, A. Mikkelsen, J.N. Andersen, J. Phys. Chem. C 113 (2009) 724.
[29] Q. Fu, W. Deng, H. Saltsburg, M. Flytzani-Stephanopoulos, Appl. Catal. B 56 (2005) 57.
[30] Q. Fu, H. Saltsburg, M. Flytzani-Stephanopoulos, Science 301 (2003) 935.
[31] M. Škoda, M. Cabala, I. Matolínová, K.C. Prince, T. Skála, F. Šutara, K. Veltruská, V. Matolín, J. Chem. Phys. 130 (2009) 034703.
[32] Z.P. Liu, S.J. Jenkins, D.A. King, Phys. Rev. Lett. 94 (2005) 196102.
[33] X. Wang, J.A. Rodriguez, J.C. Hanson, M. Perez, J. Evans, J. Chem. Phys. 123 (2005) 221101.
[34] X. Wang, J.A. Rodriguez, J.C. Hanson, D. Gamarra, A. Martínez-Arias, M. Fernández-García, J. Phys. Chem. B 110 (2006) 428.
[35] N.J. Castellani, M.M. Branda, K.M. Neyman, F. Illas, J. Phys. Chem. C 113 (2009) 4948.
[36] C. Zhang, A. Michaelides, D.A. King, S.J. Jenkins, J. Am. Chem. Soc. 132 (2010) 2175.
[37] Y.H. Tang, H. Zhang, L.X. Cui, C.Y. Ouyang, S.Q. Shi, W.H. Tang, H. Li, J.S. Lee, L.Q. Chen, Phys. Rev. B 82 (2010) 125104.
[38] P.E. Blöhl, Phys. Rev. B 50 (1994) 17953.
[39] G. Kresse, J. Furthmüller, Phys. Rev. B 54 (1996) 11169.
[40] G. Kresse, D. Joubert, Phys. Rev. B 59 (1999) 1758.
[41] J.P. Perdew, K. Burke, M. Ernzerhof, Phys. Rev. Lett. 77 (1996) 3865.
[42] S.L. Dudarev, G.A. Botton, S.Y. Savrasov, C.J. Humphreys, A.P. Sutton, Phys. Rev. B 57 (1998) 1505.
[43] S. Fabris, G. Vicario, G. Balducci, S. de Gironcoli, S. Baroni, J. Phys. Chem. B 109 (2005) 22860.
[44] N.V. Skorodumova, M. Baudin, K. Hermansson, Phys. Rev. B 69 (2004) 075401.
[45] M. Nolan, S. Grigoleit, D.C. Sayle, S.C. Parker, G.W. Watson, Surf. Sci. 576 (2005) 217.
[46] S.Q. Shi, X.Z. Ke, C.Y. Ouyang, H. Zhang, H.C. Ding, Y.H. Tang, W.W. Zhou, P.J. Li, M.S. Lei, W.H. Tang, J. Power Sources 194 (2009) 830.
[47] S.Q. Shi, Y.H. Tang, C.Y. Ouyang, L.X. Cui, X.G. Xin, P.J. Li, W.W. Zhou, H. Zhang, M.S. Lei, L.Q. Chen, J. Phys. Chem. Solids 71 (2010) 788.
[48] H.J. Monkhorst, J.D. Pack, Phys. Rev. B 13 (1976) 5188.
[49] M. Methfessel, A.T. Paxton, Phys. Rev. B 40 (1989) 3616.
[50] P.E. Blöhl, O. Jepsen, O.K. Andersen, Phys. Rev. B 49 (1994) 16223.
[51] L. Gerward, J.S. Olsen, L. Petit, G. Vaitheeswaran, V. Kanchana, A. Svane, J. Alloys Compd. 400 (2005) 56.
[52] M.V. Ganduglia-Pirovano, J.L.F. Da Silva, J. Sauer, Phys. Rev. Lett. 102 (2009) 026101.
[53] A. Kirfel, K.D. Eichhorn, Acta Crystallogr. A 46 (1990) 271.
[54] H.-Y. Li, H.-F. Wang, X.-Q. Gong, Y.-L. Guo, Y. Guo, G.-Z. Lu, P. Hu, Phys. Rev. B 79 (2009) 193401.
[55] A. Martínez-Arias, A.B. Hungría, G. Munuera, D. Gamarra, Appl. Catal. B 65 (2006) 207.
[56] Y. Liu, T. Hayakawa, T. Tsunoda, K. Suzuki, S. Hamakawa, K. Murata, R. Shiozaki, T. Ishii, M. Kumagai, Top. Catal. 22 (2003) 205.
[57] A. Hornés, A.B. Hungría, P. Bera, A.L. Cámara, M. Fernández-García, A. Martínez-Arias, L. Barrio, M. Estrella, G. Zhou, J.J. Fonseca, J.C. Hanson, J.A. Rodriguez, J. Am. Chem. Soc. 132 (2010) 34.
[58] P. Norby, R.E. Dinnebier, A.N. Fitch, Inorg. Chem. 41 (2002) 3628.
[59] J.A. Farmer, J.H. Baricuatro, C.T. Campbell, J. Phys. Chem. C 114 (2010) 17166.
[60] N.C. Hernández, R. Grau-Crespo, N.H. de Leeuw, J.F. Sanz, Phys. Chem. Chem. Phys. 11 (2009) 5246.
[61] M.F. Camellone, S. Fabris, J. Am. Chem. Soc. 131 (2009) 10473.
[62] C. Zhang, A. Michaelides, D.A. King, S.J. Jenkins, J. Chem. Phys. 129 (2008) 194708.
[63] Y. Chen, P. Hu, M.H. Lee, H. Wang, Surf. Sci. 602 (2008) 1736.
[64] M. Baron, O. Bondarchuk, D. Stacchiola, S. Shaikhutdinov, H.J. Freund, J. Phys. Chem. C 113 (2009) 6042.
[65] M.M. Branda, N.J. Castellani, R. Grau-Crespo, N.H. de Leeuw, N.C. Hernández, J.F. Sanz, K.M. Neyman, F. Illas, J. Chem. Phys. 131 (2009) 094702.
[66] G. Henkelman, A. Arnaldsson, H. Jonsson, Comput. Mater. Sci. 36 (2006) 354.
[67] B. Hammer, L.B. Hansen, J.K. Nørskov, Phys. Rev. B 59 (1999) 7413.
[68] Z. Yang, Z. Lu, G. Luo, K. Hermansson, Phys. Lett. A 369 (2007) 132.
[69] Z. Yang, Z. Lu, G. Luo, Phys. Rev. B 76 (2007) 075421.
[70] A. Bruix, K.M. Neyman, F. Illas, J. Phys. Chem. C 114 (2010) 14202.
[71] Z. Chafi, N. Keghouche, C. Minot, Surf. Sci. 601 (2007) 2323.
[72] S. Hosokawa, M. Taniguchi, K. Utani, H. Kanai, S. Imamura, Appl. Catal. A 289 (2005) 115.
[73] M. Nolan, J. Phys. Chem. C 113 (2009) 2425.
[74] J. Zhang, R.B. Von Dreele, L. Eyring, J. Solid State Chem. 104 (1993) 21.
[75] E. Shoko, M.F. Smith, R.H. McKenzie, J. Phys.: Condens. Matter 22 (2010) 223201.